A 510,000-YEAR HISTORY OF MARS' GLOBAL WATER TRANSPORT. P.B. Buhler. Planetary Science Institute (pbuhler@psi.edu)

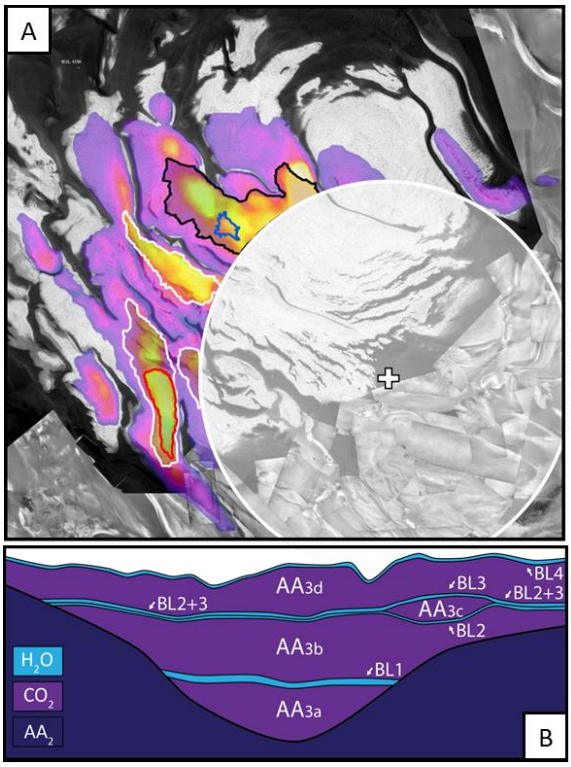

Fig. 1. A. Massive CO_2 Ice Deposit: pole (cross); no RADAR observations poleward of 87° S (white circle); 0° E (up), 90° E (right); colorized MCID thickness [1]; BL unit outlines: blue (Region 2) = "BL3" overlying "BL2", black = "BL2+3", white = "BL2+3", red (Region 1) = "BL1". On THEMIS mosaic [2] and CTX mosaic [3]. **B.** Schematic MCID cross section. AA_2 is dusty H_2O ice basement.

Introduction: Mars' polar deposits record H_2O transport between north and south polar, mid-latitude, and equatorial reservoirs in response to Mars' orbital element oscillations [4,5]. 4-5 Myr ago, a 10(+)-Myr high obliquity (ε) state favoring tropical H_2O glaciation transitioned to a low ε state [6,7]. Within <~1 Myr, tropical H_2O ice migrated to the midlatitudes and poles, followed by gradual transport of midlatitude H_2O ice to the poles [8-10]. Mars' recent (<~3.5 Myr) H_2O cycle is likely driven by 10^5-yr ε and 10^4-yr longitude of perihelion cycles. Midlatitude-to-pole H_2O transport is likely ε mediated, but quantitative present-day and historical transport rates are both highly uncertain [11]. The CO_2 south polar residual cap (SPRC) is a perennial cold-trap sink of H_2O [13].

Previous studies of polar ice H_2O ice and dust layers found ~0.1 mm yr^{-1} Myr-averaged deposition rates [14-17]. However, the rate-averaging timescale is longer than orbital cycles, the deposits have loose temporal constraints [18], and no model has yet produced a one-to-one correlation between modeled and observed layers in these deposits [10,17]. Thus, quantitative H_2O transport rates as a function of Mars' orbital configuration have remained elusive.

To address this knowledge gap, this study investigates south polar H_2O deposition rates as a function of Mars' orbital configuration in a previously unexplored record: H_2O ice layers embedded in Mars' south polar Massive CO_2 Ice Deposit (MCID; Fig. 1; [19-20]). The MCID's mass approximately equals Mars' current, principally CO_2 atmosphere [21] and has spatially variable ~10s-meter-thick H_2O ice Bounding Layers (BLs), dividing the CO_2 ice into ~100s-meter-thick layers (Fig. 1; [1]). The MCID formed through exchange between polar CO_2 ice, atmospheric CO_2, and CO_2 adsorbed in regolith, driven by Mars' cyclic ε evolution over the past 510 kyr [22-23]. When ε decreases, polar sunlight decreases, and the MCID accumulates CO_2 ice (with H_2O ice and dust impurities). When ε increases, CO_2 ablates, leaving behind lag layers (i.e., BLs) of residual H_2O ice and dust.

Previous MCID modeling assuming constant H_2O deposition [22] yielded BL thicknesses inconsistent with later observation [1]. Here, variable MCID H_2O ice deposition is modeled coupled to an MCID-atmosphere-regolith CO_2 exchange model [22-23]. Markov Chain Monte Carlo (MCMC) simulations are used to evaluate H_2O deposition rate (r_{H_2O}) functions of various orbital parameters to find the r_{H_2O} function best reproducing observed BL thicknesses.

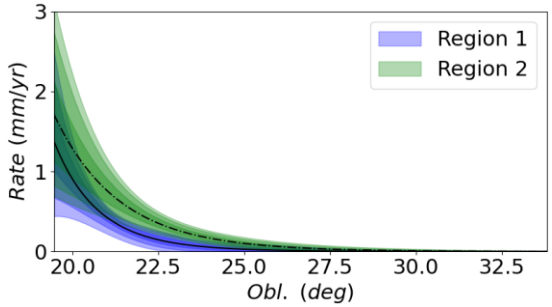

Fig. 2. Favored Region 1 (blue/solid) and 2 (green/dash-dot) models with best fit (line), 68% (dark), 95% (intermediate), and 99% (light) confidence intervals.

Methods: Model CO_2 ice flux and r_{H_2O} are calculated in 1-kyr timesteps, yielding an output 1-kyr-resolution time-marching MCID stratigraphic column. CO_2 ice flux follows equilibrated, mass-conserved MCID-atmosohere-regolith exchange, driven by ε-dependent latitudinal insolation [23]. MCID-atmosphere vapor pressure equilibrium is determined by MCID surface elevation and CO_2 ice temperature, set by insolation. Regolith-atmosphere adsorption equilibrium is determined by calculating regolith temperature, set by insolation, on a latitude-depth grid and convergently calculating atmospheric pressure and

total regolith adsorption using an empirical pressure-temperature adsorption relation [24]. The MCID and regolith exchange indirectly via the atmosphere.

A heuristic r_{H_2O} function specifies H_2O deposition. Obliquity-, eccentricity-, longitude of perihelion-, and insolation-dependent r_{H_2O} were considered, with formulations covering the range of previously proposed r_{H_2O}: polynomial and exponential [e.g., 10]; step function [e.g., 17]; cosine or gaussian (periodic or peaked [e.g., 12,25]). During CO_2 accumulation, a new model layer with appropriate fractional CO_2 and H_2O content adds to the column top. When CO_2 ablates, a pure H_2O ice layer grows at the top from both (i) newly deposited H_2O ice and (ii) previously deposited H_2O liberated from subliming CO_2. Each r_{H_2O} formulation was run through a 10^8 -iteration MCMC [23]. Model likelihoods were compared using Bayes factors, rewarding better fits but penalizing higher complexity [e.g., 26].

Models were fit to two regional observations (Fig. 1A; [1]). Region 1 is near [86° S, 270° E], clipped to where BL2+3 overlies BL1. Region 2 is near [86° S, 315° E], clipped to where BL3 separably overlies BL2; These regions are the only regions with multiple overlying BLs, and thus the only regions permitting meaningful assessment of non-constant deposition models.

Results: In Region 2, exponentially decreasing r_{H_2O}-versus-ε is strongly favored over all other models. In Region 1, exponentially decreasing r_{H_2O}-versus-ε is also strongly favored, but some other Region 1 functions have equivalent Bayes factors. However, it is difficult to conceive of processes driving r_{H_2O} according to different orbital dependencies in two nearby, physically similar environments, and other Region 1 solutions are inconsistent with process-based H_2O cycle predictions [e.g., 12,27-28]; therefore I favor equivalent Region 1 and 2 functional forms. Favored models yield Region 1 $r_{H_2O} = \exp(-0.7450 \times \varepsilon + 14.80)$ and Region 2 $r_{H_2O} = \exp(-0.5171 \times \varepsilon + 10.59)$. Model Region 1 r_{H_2O} predicts BL1 = $30.4^{+7.3}_{-6.6}$ m, BL2+3 = $28.3^{+7.3}_{-7.8}$ m, BL4 = $6.3^{+2.4}_{-2.3}$ m and present-day ($\varepsilon = 25.2°$) $r_{H_2O} = 0.03^{+0.03}_{-0.02}\ mm\ yr^{-1}$ (68% confidence; Fig. 2-3). Model Region 2 r_{H_2O} predicts BL2 = $33.8^{+7.0}_{-7.8}$m, BL3 = $25.6^{+5.0}_{-5.1}$ m, BL4 = $17.2^{+3.1}_{-3.0}$ m and present-day $r_{H_2O} = 0.09^{+0.02}_{-0.03}\ mm\ yr^{-1}$ (Fig. 2). Predicted present-day r_{H_2O} is consistent with observation [32] and physics-based models [13,28,31] and Myr-average rates from other polar stratigraphy [14-17].

Discussion: ***Regional Variation.*** Predicted regional rates of change in r_{H_2O} as a function of ε are remarkably similar, but r_{H_2O} is consistently higher in Region 2 than Region 1 (Fig. 2). Wind-mediated H_2O transport variation may cause local r_{H_2O} differences, as seen at 1-to-100-km scales in Mars polar and Antarctic (Earth) records [e.g., 29-30] and in present-day south polar r_{H_2O} observation and modeling [8,12,31]. Persistent regional variation may relate to orographic effects, e.g., asymmetrical CO_2 [32] and H_2O [31] south polar deposition driven by Hellas Basin.

Interpretation. The MCID record provides two benefits over previously analyzed dusty H_2O ice stratigraphy. First, physics-based modeling [22-23] has reproduced observed CO_2 layers, so MCID layer ages are better known than other polar layers. Second, the MCID cold traps H_2O ice, meaning (i) simpler H_2O ice depositional physics [e.g., 28] and (ii) likely negligible BL ablation [22,33], allowing deposition rate retrieval (rather than net accumulation plus ablation rates).

Mars' polar and atmospheric reservoirs are mixed on timescales shorter than ε cycles [11], so predicted ε-dependent r_{H_2O} likely probes regolith processes governing midlatitude-to-pole H_2O transport [e.g., 9]. Physics-based modeling also indicates increased midlatitude-to-pole transport with decreasing ε [8,34]. However, midlatitude ice sublimation sensitively depends on unknown regolith properties and is uncertain at order-of-magnitude levels, even for the present day [e.g., 11]. Thus, the results presented here provide a major improvement in determining quantitative ε-mediated midlatitude-to-pole H_2O transport rates.

Acknowledgments: I thank R. Alwarda and I.B. Smith for helpful discussion. Work supported by NASA Grant 80NSSC21K0212. **References:** [1] Alwarda, R., Smith, I.B., 2021. *JGR Planets* e2020JE006767. [2] Edwards, C.S. et al., 2011. *JGR Plan.* 116(E10). [3] Thomas, P.C. et al., 2016. *Icarus* 268, 118. [4] Smith, I.B. et al., 2020. *PSS* 184, 104841. [5] Becerra, P. et al., 2021. *PSJ* 2, 209. [6] Head, J.W. et al., 2003. *Nature* 426, 797. [7] Laskar, J. et al., 2004. *Icarus* 170, 343. [8] Montmessin, F. et al., 2004. *JGR Plan.* 109(E10). [9] Mellon, M.T. & Jakosky, B.M., 1995. *JGR Plan.* 100(E6). [10] Levrard et al., 2007. *JGR Plan.* 112(E6). [11] Montmessin, F. et al., 2017. in *The Atmosphere and Climate of Mars*, 338. [12] Montmessin, F. et al., 2007. *JGR Plan.* 112(E8). [13] Richardson, M.I. & Wilson, R.J., 2002. *JGR* 107, 5031. [14] Becerra. P. et al., 2017. GRL 44(1), 62. [15] Becerra, P. et al., 2019. GRL 46, 7268. [16] Sori, M.M. et al., 2022. GRL e2021GL097450. [17] Hvidberg, C.S. et al., 2012. *Icarus* 221(1), 405. [18] Tanaka, K.L. et al., 2008. *Icarus* 196(2), 318. [19] Phillips, R.J. et al., 2011. *Science* 332, 838–841. [20] Bierson, C. et al., 2016. *GRL* 43, 4172–4179. [21] Putzig, N.E. et al., 2018. *Icarus* 308, 138. [22] Buhler, P.B. et al., 2020. *Nat. Astro.* 4, 364-371. [23] Buhler, P.B. & Piqueux, S., 2021. *JGR Plan.* 126, e2020JE006759. [24] Zent, A.P. & Quinn, R.C., 1995. *JGR* 100, 5341. [25] Vos, E. et al., 2019. *Icarus* 324, 1. [26] Kass, R.E. & Raftery, A.E., 1995. *J. Am. Stat. Asc.* 90, 773. [27] Toon, O.B. et al., 1980. *Icarus* 44, 552. [28] Mischna, M.A. et al., 2003. *JGR Plan.* 108(E6) [29] Smith, I.B. et al., 2013. *JGR Plan.* 118, 1835 [30] Herny, C. et al., 2014. *EPSL* 403, 55. [31] Langevin, Y. et al., 2007. *JGR Plan.* 112(E8). [32] Colaprete, A. et al., *Nature* 435, 184. [32] Brown, A.J. et al., 2014. *EPSL* 406, 102. [33] Innanen, A.C. et al., 2022. *PSJ* 3, 242. [34] Schorghofer, N. & Forget, F., 2012. *Icarus* 220, 1112.